# Characterization of the Sr²⁺- and Cd²⁺-Substituted Oxygen-Evolving Complex of Photosystem II by Quantum Mechanics/Molecular Mechanics Calculations

Fabio Pitari, Daniele Bovi, Daniele Narzi, and Leonardo Guidoni*

University of L'Aquila, 67100 L'Aquila, Italy

ABSTRACT: The Mn_4CaO_5 cluster in the oxygen-evolving complex is the catalytic core of the Photosystem II (PSII) enzyme, responsible for the water splitting reaction in oxygenic photosynthesis. The role of the redox-inactive ion in the cluster has not yet been fully clarified, although several experimental data are available on Ca^{2+}-depleted and Ca^{2+}-substituted PSII complexes, indicating Sr^{2+}-substituted PSII as the only modification that preserves oxygen evolution. In this work, we investigated the structural and electronic properties of the PSII catalytic core with Ca^{2+} replaced with Sr^{2+} and Cd^{2+} in the S_2 state of

the Kok−Joliot cycle by means of density functional theory and ab initio molecular dynamics based on a quantum mechanics/molecular mechanics approach. Our calculations do not reveal significant differences between the substituted and wild-type systems in terms of geometries, thermodynamics, and kinetics of two previously identified intermediate states along the S_2 to S_3 transition, namely, the open cubane S_2^A and closed cubane S_2^B conformers. Conversely, our calculations show different pK_a values for the water molecule bound to the three investigated heterocations. Specifically, for Cd-substituted PSII, the pK_a value is 5.3 units smaller than the respective value in wild type Ca-PSII. On the basis of our results, we conclude that, assuming all the cations sharing the same binding site, the induced difference in the acidity of the binding pocket might influence the hydrogen bonding network and the redox levels to prevent the further evolution of the cycle toward the S_3 state.
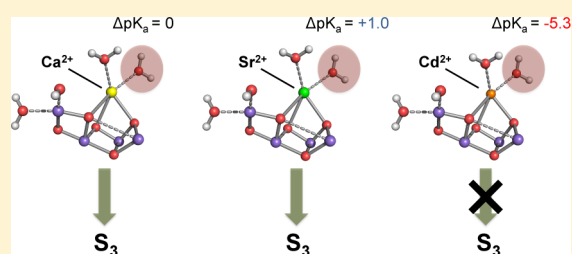
For 2.5 billion years, plants, algae, and cyanobacteria have used the Photosystem II (PSII) complex to capture light energy from the sun and convert it into chemical energy.[1] A crucial step in the natural oxygenic photosynthetic process lies in the water splitting reaction occurring along the five steps $(S_0−S_4)$ of the Kok−Joliot cycle.[2] The energy necessary to perform this catalytic step is absorbed from the sun by the antenna system (i.e., a system of light-absorbing protein−pigment complexes) and transferred to the reaction center of the PSII complex. In this site, the oxidation of two water molecules is catalyzed by the manganese−calcium (Mn_4CaO_5) cluster after the photoinduced removal of four electrons from the complex itself.

Beyond its fundamental relevance to biology, a deep understanding of the molecular details behind the photosynthetic water splitting mechanism may also serve as inspiration for the development of artificial devices that can convert solar energy into chemical green fuels such as molecular hydrogen.[3−7] In the past decade, atomic details of the structure of PSII have been revealed at an increasing level of accuracy.[8−14] However, only in 2011 did a high-resolution (1.9 Å) X-ray structure become accessible,[15] thus providing the bases for accurate computational investigations of the catalytic function of PSII.[16−20] Additionally, a new radiation damage-free crystal structure, supposed to be representative of the S_1 state of the Kok−Joliot cycle, has been reported[21] in the past year.

In particular, the role of the calcium ion present in the Mn_4CaO_5 complex of PSII was largely debated after direct

observations of its involvement in the O_2 evolution mechanism.[22] To understand the role played by Ca^{2+} in the water splitting mechanism, several experiments based on Ca^{2+} depletion or substitution with other ions (mainly divalent cations and alkali metals)[23−31] as well as theoretical studies[32−36] were conducted.

No catalytic activity was shown for the Ca^{2+}-depleted PSII, whereas its substitution with the Sr^{2+} ion is capable of largely restoring O_2 production,[37] albeit with O_2 evolving activity reduced by 40−50% with respect to that of wild-type PSII.[38] The functional similarity between Sr^{2+}- and Ca^{2+}-PSII corresponds to a structural similarity, as revealed by a recent crystal structure of Sr-substituted Photosystem II[38] at 2.1 Å resolution. The overall chemical structure of the region around the catalytic site is sketched in Figure 1a. The differences between Ca^{2+}- and Sr^{2+}-PSII are only minor rearrangements in the oxygen-evolving complex region with the relevant exception of the W3 water oxygen, which is shifted away from the Sr^{2+} ion by ∼0.3 Å. Crystallographers suggested that such a difference, together with the cubane distortion, might explain the decreased rate of O_2 production, because the W3 water molecule is not maintained in some specific position that may be required for the catalytic mechanism.[38] On the basis of this experimental evidence, the catalytic role of the Ca^{2+} ion was
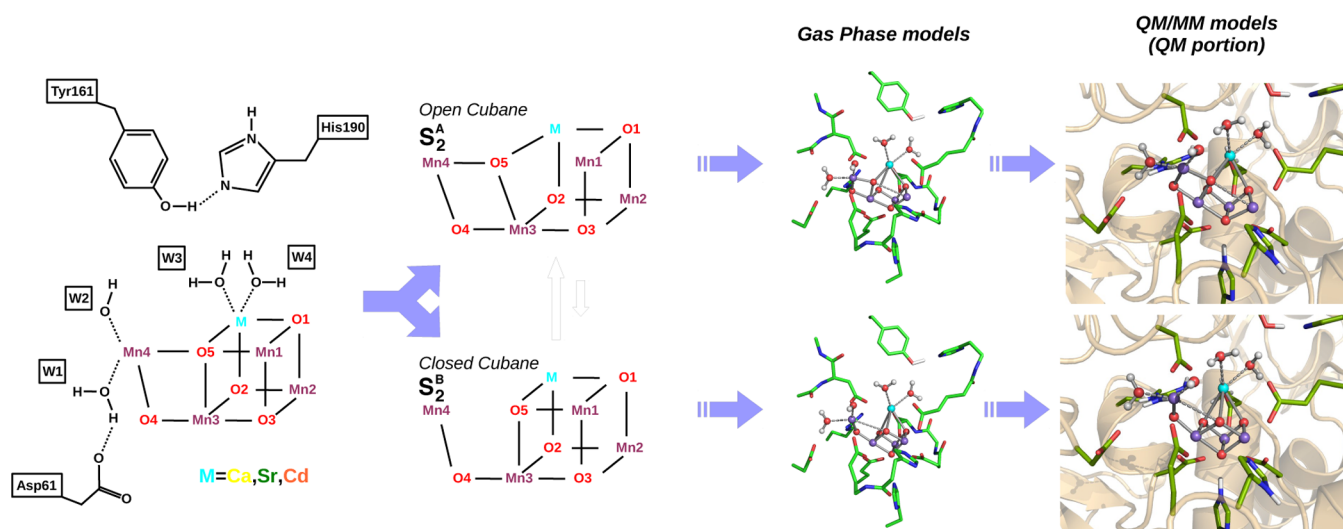
Figure 1. Scheme of the studied systems. The left panels show a sketch of the metal−oxo cluster (Mn_4MO_5, where M represents the heterocation) with the most relevant residues and water molecules involved in the catalytic mechanism of PSII. The two conformers representative of the S_2 state of the Kok−Joliot cycle (namely, S_2^A and S_2^B) are also shown. The right panels show selected atoms of the catalytic center of PSII in both S_2^A and S_2^B conformations used for the density functional theory calculations in the gas phase and QM/MM calculations. The Mn_4MO_5 cluster is represented as balls and sticks, while the other residues included in the QM part are shown as sticks. The portion of the system treated at the MM level is shown in cartoon representation.

suggested to be not merely structural; it should also have functional implications.[22,33,38,39] Additionally, the W3 water molecule itself may participate as a substrate molecule in the oxygen evolution reaction.[40]

In contrast with the case of the Sr-substituted PSII complex, the substitutions with monovalent cations, such as K^+, Rb^+, and Cs^+ were not to be able to restore the O_2 evolution activity. More severely, these ions seem to block the catalytic cycle in an early stage, because no EPR signals corresponding to the S_2 state have been reported.[25]

The substitution with Cd^{2+} is also blocking the catalytic activity,[26] although its actual displacement is still a matter of debate. Several experiments have been performed to study the binding site of the Cd^{2+} ion within PSII[24,26,41−47] and within the bacterial reaction center.[48−51]

In Cd-substituted experiments, Sigfridsson et al.[52] did not observe the multiline EPR signal of the S_2 state, also identifying additional Cd^{2+} binding sites in PSII. Others experiments suggest that the cadmium cation replaces the calcium cation in the same position.[24,41−43] More recently, Lee et al. were able to detect a multiline EPR signal in the S_2 state for the Cd^{2+}-inhibited PSII by a 200 K illumination of a dark-adapted sample.[29]

The effect of the ion substitution or depletion on the S_2 to S_3 transition was also studied by means of thermoluminescence experiments.[26] In the Ca-depleted samples, the amplitude of the peak arising from $S_2Q_B^-$ was upshifted and did not further oscillate after two flashes. Interestingly, that peak was restored with the insertion of both Sr^{2+} and Cd^{2+}, whereas the oscillation was damped with the former and completely absent with the latter. In summary, these results showed that the S_2 to S_3 transition is inhibited by Ca^{2+} depletion and by Ca^{2+} substitution with the Cd^{2+} ion, and only partially recovered by repletion with the Sr^{2+} ion.

Recently, the existence of two distinct structural conformers of the Mn_4CaO_5 cluster representative of the S_2 state of the Kok−Joliot cycle was proposed.[53] One of the two conformers (namely, the S_2^A model) is characterized by an open cubane

(OC) structure (see Figure 1) and an $S = \frac{1}{2}$ spin ground state, consistent with the EPR multiline signal. The other conformer (namely, the S_2^B model) has an $S = \frac{5}{2}$ ground state consistent with the EPR signal at $g = 4.1$ and characterized by a closed cubane (CC) conformation (see Figure 1). The two conformers were found to be interconvertible at physiological temperature,[54] and the transition from the S_2 state to the S_3 state was suggested to proceed passing first by the S_2^A state and afterward through the S_2^B state.[55] On the basis of EPR measurements, Boussac et al.[56] revealed that the $g = 4.1$ signal, corresponding to the closed cubane configuration, is present also in Sr-substituted PSII. Conversely, in the Cd-substituted PSII complex, the typical double EPR signal associated with the S_2 state was not found. Despite the massive amount of available experimental and theoretical data, the effect of the replacement of Ca^{2+} with Sr^{2+}, or Cd^{2+}, in the S_2 to S_3 transition is not completely understood. Whereas Sr^{2+}-substituted PSII is supposed to behave like Ca^{2+}-PSII, from structural and electronic points of view, the effect of the substitution of calcium with the Cd^{2+} ion might be more severe.

One possibility is that the replacement of the Ca^{2+} with the Cd^{2+} ion could inhibit the interconversion between the two S_2 conformations, suggested to be necessary for the transition to the S_3 state.[55] Another hypothesis is that the Cd^{2+} ion is characterized by a Lewis acidity out of the range required for catalytic activity.[24,39] In this respect, because of the different chemical nature of the ions, the hydrogen bonding network and the proton displacement in the binding pocket might be different when different divalent cations bind to the cluster. Moreover, the heterocation substitution, affecting the electronic structure of the cluster, could have a significant influence on the redox potential of either the Tyr-Z[57] or the cluster itself[58] or else modulate oxygen release.[59]

In this work, by means of gas-phase quantum mechanics (GP) and mixed quantum mechanics/molecular mechanics (QM/MM) calculations, we compared the geometries, electronic properties, and pK_a values of the Sr/Cd-substituted complexes with respect to those of the wild-type form using

Table 1. Comparison of the Main Distances (angstroms) in the Metal–Oxo Cluster between the XRD Structure and the Optimized S_2^A and S_2^B Conformers[a]

model	Mn4–O5	Mn1–O5	MO5	MO1	MO2	M–D171	M–D143	M–W3	M–W4
Ca(S_2^A)-GP	1.93	3.17	2.71	2.46	2.57	2.43	2.57	2.36	2.44
Ca(S_2^A)-QMMM	1.87	2.98	2.49	2.38	2.63	2.39	2.49	2.47	2.34
Ca(S_2^B)-GP	3.27	1.84	2.71	2.54	2.57	2.44	2.61	2.39	2.41
Ca(S_2^B)-QMMM	3.07	1.86	2.55	2.49	2.55	2.43	2.48	2.48	2.34
crystal structure	2.50	2.60	2.49	2.33	2.49	2.44	2.54	2.39	2.49
model	Mn4–O5	Mn1–O5	MO5	MO1	MO2	M–D171	M–D143	M–W3	M–W4
Sr(S_2^A)-GP	1.85	3.25	2.82	2.54	2.68	2.57	2.59	2.52	2.56
Sr(S_2^A)-QMMM	1.87	3.06	2.57	2.50	2.70	2.54	2.64	2.63	2.47
Sr(S_2^B)-GP	3.23	1.84	2.83	2.58	2.68	2.58	2.63	2.56	2.59
Sr(S_2^B)-QMMM	3.12	1.86	2.61	2.55	2.66	2.53	2.68	2.61	2.46
crystal structure	2.53	2.68	2.62	2.46	2.67	2.73	2.59	2.74	2.27
model	Mn4–O5	Mn1–O5	MO5	MO1	MO2	M–D171	M–D143	M–W3	M–W4
Cd(S_2^A)-GP	1.84	3.16	2.78	2.36	2.52	2.36	2.54	2.32	2.32
Cd(S_2^A)-QMMM	1.88	3.01	2.46	2.39	2.57	2.36	2.57	2.44	2.31
Cd(S_2^B)-GP	3.16	1.85	2.75	2.43	2.48	2.37	2.71	2.33	2.32
Cd(S_2^B)-QMMM	3.11	1.86	2.57	2.48	2.52	2.36	2.58	2.40	2.32
crystal structure	–	–	–	–	–	–	–	–	–

[a]Calculations were performed in gas-phase and QM/MM models, optimizing the systems in their respective spin ground states, for all three studied heterocations. Distances between the heterocation and the two ligands, Asp143 and Asp171, and between the heterocation and the two coordinated water molecules, W3 and W4, are also reported.

geometry optimizations and molecular dynamics simulations. The aim of our work is to characterize the two substitutions, evaluating the different hypotheses proposed so far to interpret the experimental data.

METHODS

Gas-Phase (GP) Models. The gas-phase model of the oxygen-evolving complex active core consists of 238 atoms, including the manganese cluster, its closest residues (Asp61, Tyr161, His190, CP43-Arg357, and His337), and the water molecules present in that area, namely, two water molecules bound to the divalent ion, two bound to the Mn4, and eight crystallographic water molecules nearby. To prevent structural distortion due to the lack of the protein environment, the terminal heavy atoms at the external shell of the system were constrained in the crystallographic position. The protonation states of these systems in the S_2 catalytic step were chosen as suggested by previous studies.[54,60,61] We performed geometry optimizations for GP Ca-, Sr-, and Cd-PSII model systems in both the open (S_2^A) and closed (S_2^B) cubane conformations, using density functional theory (DFT) by means of the ORCA package[62] with the B3LYP hybrid functional[63–65] with the TZVP basis set[66] and def2-TZVP/J auxiliary basis set[67] for all atoms. An implicit solvent model (COSMO)[68] with a dielectric constant $\varepsilon = 8$ and the zero-order regular approximation (ZORA)[69] for scalar relativistic corrections were also included in the calculations.

QM/MM Models. In quantum/classical models, we have considered a QM region around the Mn_4CaO_5 cluster of 224 atoms embedded in a portion of PSII solvated in liquid water treated by classical force fields (further details in ref 61). The atomic coordinates and the protonation pattern were chosen in a manner consistent with previous theoretical studies of the manganese cluster.[53,54,60,61] The Ca-substituted QM/MM systems were termed Cd-PSII and Sr-PSII and considered in both the open (S_2^A) and closed (S_2^B) cubane conformations. The QM/MM calculations were performed using the CP2K package[70,71] with the Gaussian and plane-wave (GPW) basis

set combination. We have used GTH pseudopotential[72,73] with the DZVP Gaussian basis set and with plane-wave.[74] In both QM/MM geometry optimization and molecular dynamics calculations, we adopted a PBE+U scheme[75–77] as reported in ref 61, while the kinetic energy cutoff for plane-wave basis set expansion was 380 Ry for geometry optimizations and 320 Ry for molecular dynamics. In QM/MM geometry optimizations, only the positions of the QM atoms were optimized, the MM part being fully constrained. In MD simulations, the C_α atoms of the protein atoms treated classically were kept fixed at their X-ray positions. MD calculations were performed in the NVT ensemble, with a 0.5 fs time step and a Nosé–Hoover thermostat[78–80] with a temperature equal to 298 K; 6 ps productions were performed after thermalization for 3 ps. Projected density of states (PDOS) calculations were performed on three QM/MM models, Ca-, Sr-, and Cd-PSII, in the two optimized configurations, i.e., open (S_2^A) and closed (S_2^B) cubane, for different positions of the proton shuffling between the W1 water molecule and Asp61 (see Figure 1). Following the suggestions of Siegbahn,[81] PDOS analysis was conducted using the B3LYP* hybrid functional[63–65] with 15% HF exchange.

RESULTS AND DISCUSSION

In this study, we systematically investigate the effect of the Ca^{2+} substitution in the Mn_4CaO_5 cluster on the structure, thermodynamics, and electronic properties of the cluster in the S_2 state of the Kok–Joliot cycle. First, the structures of the two conformers representative of the S_2 state were analyzed for the different substituted systems using DFT calculations on both gas-phase and QM/MM models. Because the interconversion between the open cubane and closed cubane configurations is supposed to be relevant for the transition between S_2 and S_3 states,[53,54,82] we have also investigated whether the metal substitution affects the relative stabilities of the two conformers (S_2^A and S_2^B) and the interconversion energy barrier. Moreover, because the transfer of the electron to the radical Tyr-Z turned out to be more favorable from the S_2^B
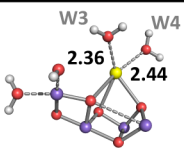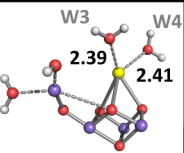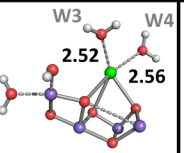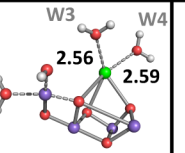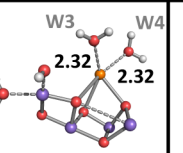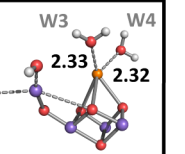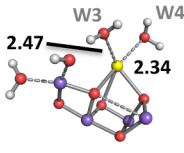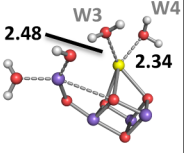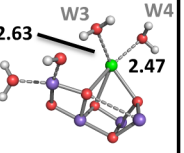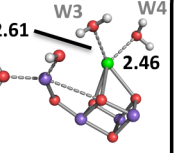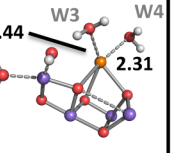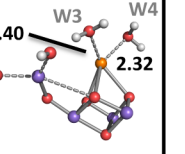
Figure 2. Characterization of the heterocation−water molecule distances. The distances between the heterocation and the two coordinated water molecules (namely, W3 and W4) calculated by gas-phase and QM/MM calculations are shown for both the S_2^A and S_2^B conformations. The Mn_4MO_5 cluster and the coordinated water molecules are represented by balls and sticks.

state,[55] possible electron structure differences in the conformers were investigated. In this respect, we have also explored the effects of the substitutions on the electron structure of the system, focusing on the capability of the manganese cluster to reduce the radical Tyr-Z through the analysis of the projected density of states (PDOS). Additionally, the QM/MM molecular dynamics of the Sr- and Cd-substituted PSII complex in the S_2 state after the removal of an electron was performed and compared with the dynamics of the wild-type form investigated in a recent work.[55] Finally, the pK_a values of the water molecule bound to the Ca^{2+}, Sr^{2+}, and Cd^{2+} ions coordinated to the manganese cluster were evaluated in their local protein environment by *ab initio* calculations.

Geometrical Characterization of the Manganese Cluster. To check the effect of the substitution of the calcium ion on the geometrical properties of the manganese cluster in the S_2 state of the Kok−Joliot cycle, we performed DFT calculations on the three Mn_4MO_5 (M = Ca, Sr, and Cd) systems in both the S_2^A (open cubane) and S_2^B (closed cubane) conformers. A first set of calculations has been conducted using a gas-phase model that includes the atoms of the manganese cluster and of the closest amino acids and water molecules [see Gas-Phase (GP) Models for details]. The most relevant distances (e.g., Mn−O5, M4−O5, and M^{2+}−ligands) are reported in Table 1, while in Figure 2, the structures of the six investigated systems are shown, highlighting the distances between the heterocation and the two coordinated water molecules. The distances for the Mn_4CaO_5 cluster reported in Table 1, calculated on the GP model, show a good agreement with those computed in previous theoretical studies for both the closed and open cubane conformations.[53,54] In particular, the distances between the calcium ion and the W3 and W4 water molecules seem not to be affected by the different conformation of the cluster (see also Figure 2) with a Ca−W4 distance slightly larger than the Ca−W3 distance. Similar observations can be made in the case of the Mn_4SrO_5 and Mn_4CdO_5 clusters. Also, in these cases, the distances between the two W3 and W4 water molecules and the heterocation are rather insensitive to the conformation adopted by the cluster. Nevertheless, when compared to those of the Ca-substituted system, both distances were found to be increased by more than 0.1 Å in the case of the Sr substitution, whereas a shortening of the two distances with respect to those of the Mn_4CaO_5 cluster was observed in the case of the Cd

substitution. In particular, the W4−Cd distance was found to be ∼0.1 Å shorter than the respective distance in the Mn_4CaO_5 cluster.

A second set of calculations has been performed in a QM/MM framework (see QM/MM Models for details), and the calculated distances are reported in Table 1. For the open and closed cubane conformations, we found that the explicit inclusion of the protein environment in the calculation results in an elongation of the W3−heterocation distance and a decrease in the W4−heterocation distance. This behavior is more evident in the Ca- and Sr-substituted clusters, whereas in the Cd-substituted system, the increase in the W3−Cd distance is not associated with a clear decrease in the W4−Cd distance. In summary, our QM/MM calculations, in contrast to the gas-phase calculations, predict for all the investigated systems a W3−cation distance longer than the W4−cation distance. Moreover, such distances in the case of the Sr-substituted cluster were found to be larger than the respective distances in the Mn_4CaO_5 cluster and in the Mn_4CdO_5 model system.

It has to be pointed out that, even though X-ray structures for the wild type[15,21] and the Sr-substituted PSII[38] are available, no tight comparisons between our calculations and the available structures can be done quantitatively, because of the different S catalytic step detected by the X-ray experiment (largely populated in the S_1 state[21]) and the issues regarding its radiation damage.[15,36,60] In this respect, the computed distances of our M-substituted models are not varying significantly between the metals.

From the point of view of the local rearrangements of the surrounding water molecules and ligands, the effect of the substitution is therefore minimal. If the Cd^{2+} ion is therefore binding in the same site of the Ca^{2+} ion, we may exclude the possibility that its inactivity arises from a different rearrangement of its ligands.

Thermodynamics and Kinetics of the Open−Closed Cubane Transition. Because the thermodynamics and the kinetics of the S_2^A (open cubane) to S_2^B (closed cubane) transition were shown to be relevant for the passage to the S_3 state,[54,55] we have investigated the effects of the substitution of the calcium ion along the energy profile characterizing the interconversion between the closed and open cubane isomers. The calculated energy differences between the two conformers in gas-phase models were found to be −3.3 kcal/mol for the Mn_4CaO_5 cluster, −2.3 kcal/mol for the Mn_4SrO_5 cluster, and
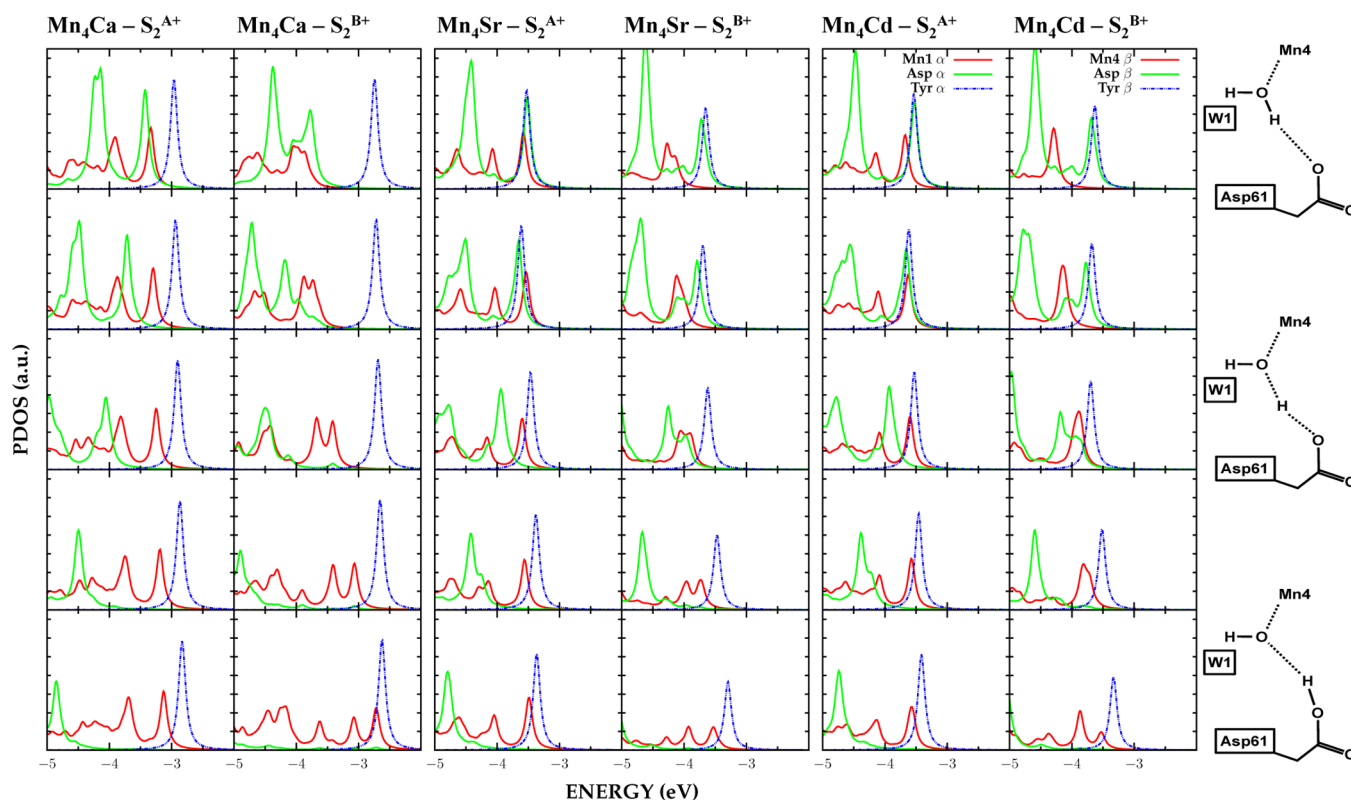
Figure 3. Projected density of states along W1−Asp61 proton exchange. Influence of the position of the proton shuffling between Asp61 and the W1 water molecule on the density of states of molecular orbitals projected on the relevant moieties involved in the PCET mechanism calculated in the oxidized S_2^+ state. The calculations were performed considering different positions of the proton for the open and closed cubane conformers in the presence of Ca^{2+}, Sr^{2+}, and Cd^{2+}. Occupied states are represented as solid lines [green for projection on Asp61 and red for projection on Mn(III), i.e., Mn1 in the S_2^A conformer and Mn4 in the S_2^B conformer]. The unoccupied state, corresponding to the LUMO localized on the Tyr-Z, is represented as a blue dashed line.

−4.1 kcal/mol for the Mn_4CdO_5 cluster. In all cases, the open cubane structure turns out to be energetically more stable than the closed cubane structure. In a previous work,[54] we also estimated the free energy difference between the two isomers within QM/MM finite temperature thermodynamic integration to be close to −1 kcal/mol for the Mn_4CaO_5 cluster with an activation barrier of 10.6 kcal/mol. An estimate of the enthalpic contribution of such a barrier can be made by calculating energies for different positions of the O_5 atom along a reaction coordinate constraining the distance between O_5 and the two manganese ions (Mn1 and Mn4) while optimizing all the resto of the geometry. The maximal value of the energy corresponds to 2.25 Å for both the Mn1−O_5 and Mn4−O_5 distances, and for this conformer, the energy difference with respect to the open cubane isomer was evaluated to vary between 14 and 15 kcal/mol for all the three studied systems. The overestimation of the energy barrier when compared with the value found for the Mn_4CaO_5 cluster investigated in ref 54 can probably be ascribed to the entropic contribution not taken into account in the current static calculation. Nevertheless, because of the similar dynamic behavior of the three systems, a similar entropic contribution for the Mn_4CaO_5 cluster and the two substituted clusters can be assumed. In summary, the estimated activation energy for the interconversion between the open and closed cubane isomers clearly suggests that the rate of transition between the two conformers is not significantly affected by the nature of the heterocation present in the manganese cluster, assuming that the substituting cations occupy the Ca^{2+} ion position.

Structural and Electron Characterization of the Mn(III) Oxidation. In a recent study,[55] we observed that the proton shuffling between the W1 molecule and the neighbor Asp61 modulates the reduction of the radical Tyr-Z by the Mn4(III) in the closed cubane structure during the S_2 to S_3 transition. The observed proton coupling electron transfer (PCET) mechanism was conversely not observed starting from the open cubane conformation along 10 ps of free QM/MM MD simulation. These observations suggest different electronic structure properties of the two conformers. Such properties might also, in principle, be influenced by the nature of the divalent cation of the cluster that can therefore inhibit or promote the oxidation of the manganese cluster by Tyr-Z. In this section, we report additional details of the analysis of the electron structure of the cluster to rationalize the differences between the closed and open cubane conformations, as well as the differences between the substituents.

A good reaction coordinate to follow such event is the proton transfer between W1 and Asp61, which, as observed in our previous study,[55] is concomitant with the electron transfer between the Mn(III) (namely Mn1 in the open cubane and Mn4 in the closed cubane structure) and the Tyr-Z. As a function of this reaction coordinate, we have here monitored the energy levels of the electrons by means of calculating the projected density of states (PDOS) on the different residues and ions involved in the PCET mechanism (see also Figure 1). The calculations were performed for the six studied systems [two conformations for each investigated heterocation, namely Ca(S_2^A), Ca(S_2^B), Sr(S_2^A), Sr(S_2^B), Cd(S_2^A), and Cd(S_2^B)] in the S_2
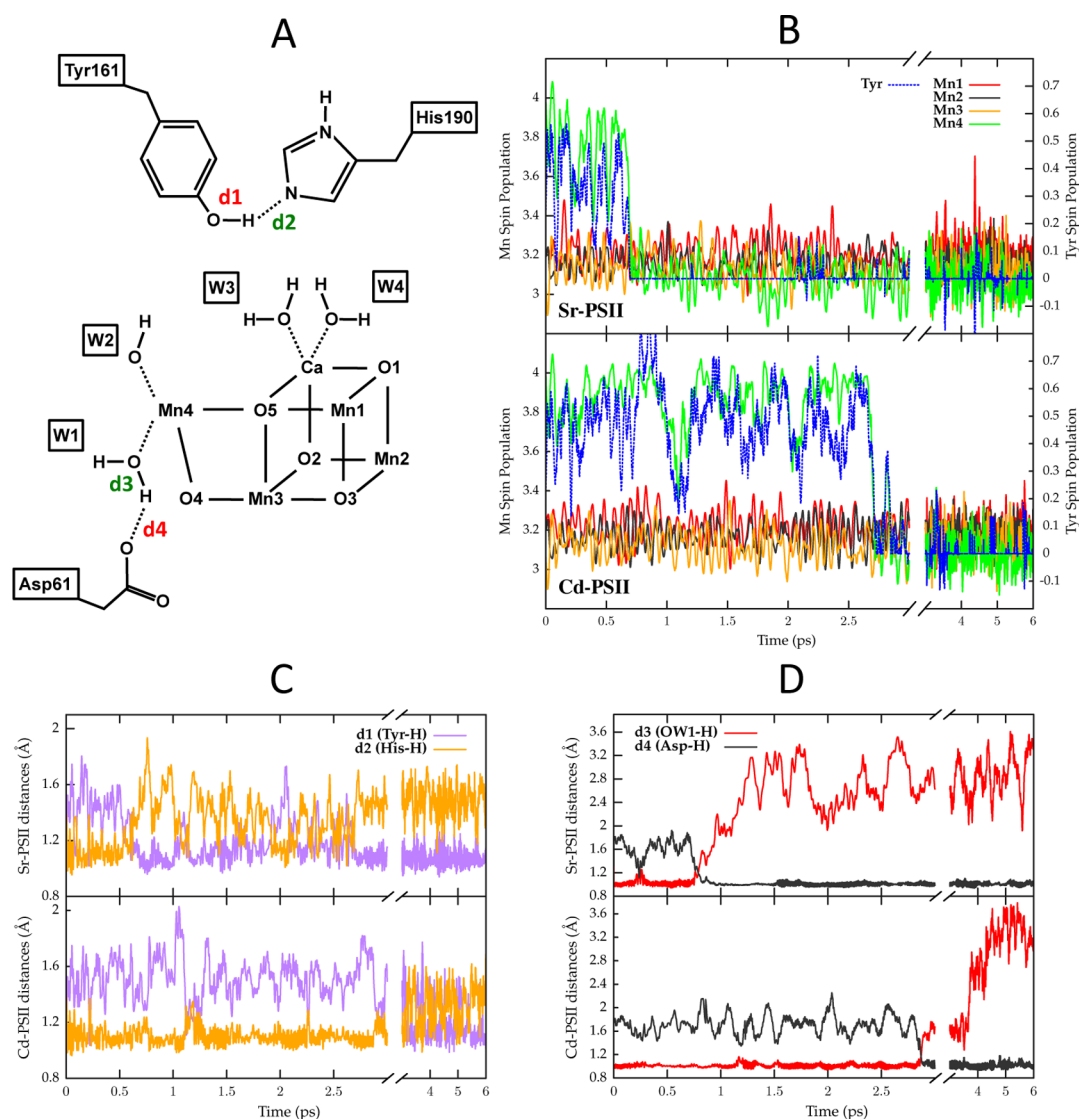
Figure 4. QM/MM molecular dynamics of the Sr- and Cd-substituted cluster in the S_2^{B+} state. (A) Sketch representing the Mn_4CaO_5 cluster, the three residues Asp61, Tyr161, and His190, and the four coordinated water/hydroxide molecules highlighting the four distances (d_1-d_4) characterizing the PCET mechanism. (B) Spin populations of the four Mn ions (solid lines, left scale) and Tyr-Z (dashed line, right scale) reported as a function of the simulation time for the Sr- and Cd-substituted clusters. In both cases, the oxidation of Mn4(III) by the radical Tyr-Z was found to occur in <3 ps. (C) Time evolution of distances d_1 and d_2. (D) Time evolution of distances d_3 and d_4. The distance analysis shows the prevalent protonation of Tyr-Z after the electron transfer and the occurrence of a simultaneous proton transfer from water molecule W1 to Asp61.

state after the removal of one electron (i.e., S_2^+ state). For each case, we focus on the relative energies between the HOMO, describing the electron of the Mn(III) ion highest in energy, and the LUMO localized on the Tyr-Z radical (shown in Figure 3). The PDOS referred to the proper atoms and distinguished the density of the occupied (solid line) from the unoccupied (dashed line) states. In a manner consistent with the previous study,[55] in the open cubane structure in the presence of calcium ion, we observe the HOMO and LUMO from the PDOS on the Mn1 ion and Tyr-Z, respectively, remaining unchanged along the reaction coordinate (see the first column in Figure 3). This behavior reflects the tendency of the electron to be removed from the Tyr-Z with a radicalization of the tyrosyl group and no further electron transfer from Mn1 to the Tyr-Z. In contrast in the closed cubane structure (see the second column in Figure 3), the relative energies of the HOMO and LUMO localized on the Mn4 ion and Tyr-Z change while the proton, originally on water molecule W1, is moved to Asp61. In

particular, when Asp61 is protonated, the PDOS on Mn4 and Tyr-Z shows an evident overlap of the HOMO and LUMO densities that can promote the oxidation of Mn4(III) by the radical tyrosyl group. Notably, in the open and closed cubane models, the HOMO projected on the Asp61 (solid green line in Figure 3) is stabilized by the protonation of the aspartic acid.

As in the case of the Mn_4CaO_5 cluster, for the Sr- and Cd-substituted open cubane models, the relative positions of the PDOS of Mn_1(III) and Tyr-Z are not strongly affected by the protonation state of Asp61 (see the third and fifth columns in Figure 3). Additionally, also in these two cases, the density of the highest occupied state projected on the Asp61 moves to lower energies while the proton is moved from the W1 water molecule to Asp61. It has to be pointed out that, in contrast with the calcium case, in the presence of Sr^{2+} or Cd^{2+} ion the LUMO on Tyr-Z and the HOMO on the Mn4 ion show evident overlap. In the closed cubane model, for the Sr- and Cd-substituted clusters, the positions of the PDOS of Mn4(III)

and Tyr-Z are modified by the position of the proton of the W1 water molecule (see the fourth and sixth columns in Figure 3). In particular, when Asp61 is protonated, the LUMO localized on the Tyr-Z and the HOMO localized on the Mn4 ion show clear overlap as in the presence of the calcium ion in the cluster. This behavior is consistent with the possible fast oxidation of Mn4(III) to Mn4(IV) by the tyrosyl group. In contrast, when the proton is localized on the W1 water molecule, the two orbitals mentioned above appear distant in energy by ~1 eV. Our results suggest that, as in the case of the Mn_4CaO_5 cluster, the protonation state of Asp61 regulates the oxidation of Mn4(III) by Tyr-Z in the closed state configuration for both the Sr-substituted cluster and the Cd-substituted test model. Conversely, in the open cubane state isomer, no clear dependence on the protonation state of Asp61 was found for the relative positions of the PDOS related to Mn1(III) and Tyr-Z. We can conclude that from the PDOS analysis the oxidation of Mn(III) by the radical Tyr-Z in the S_2 state seems not be significantly perturbed or inhibited by the substitution of the calcium ion with Sr or Cd.

We can also point out that both substitutions were shown to affect the position of the LUMO projected on Tyr-Z with respect to the states of the Mn_4CaO_5 cluster. In particular, the energy corresponding to this orbital is lower in the substituted systems than in the case of Mn_4CaO_5 for the open and closed cubane models. We can speculate that the influence of the divalent ion on the environment around Tyr-Z might affect the localization of the orbitals on the tyrosyl group, thus modulating the oxidation potential of Tyr-Z, as already suggested by Pantazis and co-workers.[57]

To verify the possibility of the oxidation of Mn4(III) by the radical Tyr-Z in the closed cubane isomer, we performed unconstrained QM/MM molecular dynamics simulations for the Sr- and Cd-substituted systems in the S_2 state after the removal of one electron from the system, which is similar to what we did previously for Ca-PSII.[55] In Figure 4B, we show the Mulliken spin populations of the four Mn ions and Tyr-Z as a function of time for both simulated systems.

For the Sr-substituted cluster, the tyrosyl group of Tyr-Z was found in its radical state in the first 0.7 ps of the simulation while the four Mn ions keep their starting spin populations expected for the S_2 state of the Kok–Joliot cycle. After 0.7 ps, a concerted transition of the spin populations of Mn4 and Tyr-Z occurs, which leads to the oxidation of Mn4 and the reduction of Tyr-Z. The effect of such electron transfer is the modification of the overall oxidation state of the Mn_4SrO_5 cluster into an electronic configuration consistent with the S_3 state of the Kok–Joliot cycle. As in the case of the Mn_4CaO_5 cluster (previously investigated in a recent work[55]), the electron transfer was found to have a strong correlation with the proton exchange between Asp61 and water molecule W1 (Figure 4A,D). The simultaneous formation of a hydroxide ion in place of the W1 water molecule and protonation of Asp61 occur in parallel with the oxidation of Mn4(III). Additionally, after the transfer of an electron from Mn4 to Tyr-Z, the protonation state of His190 and Tyr-Z was inverted, with the proton binding to the tyrosyl oxygen and His190 in its deprotonated state (see Figure 4B). A similar behavior was found in the case of the test model with the cadmium ion in place of the calcium. Here the oxidation of Mn4(III) by the radical Tyr-Z was found to occur after simulation for 2.6 ps. Nevertheless, the protonation of Asp61 and the W1 water molecule and the

protonation of His190 and Tyr-Z were found to follow the same path shown in the Mn_4SrO_5 and Mn_4CaO_5 systems.

These results, which are consistent with the PDOS analysis, show that the substitution of the calcium ion with strontium or cadmium does not inhibit the oxidation of Mn4(III) by Tyr-Z in the closed cubane structure.

If we assume that Cd^{2+} occupies in the S_2 state the same binding site occupied by the Ca^{2+} ion in wild-type PSII, as supported by experiments,[39] our calculations would show that there are no electronic or structural reasons that would prevent the system from proceeding toward the S_3 state under the conditions employed in the simulation. Nevertheless, our calculations assume that the hydrogen bond and the protonation pattern of the binding pocket, when the Cd^{2+} ion is bound, are exactly the same as those found in wild-type PSII. This assumption would turn out to be incorrect if the protonation of bound water molecules and the acidity of the binding pocket were altered by the metal substitution. This issue will be addressed in the next paragraph.

Relative Acidity of the Heterocations. It was suggested that one reason for the various activities of different heterocations placed in the Ca^{2+} binding site may lie in their own acidity, i.e., different pK_a values of the metal-aqua ion coordinated with the heterocation.[24,39] The values of pK_a for the Ca^{2+}-aqua ion and Sr^{2+}-aqua ion are similar (pK_a-Ca^{2+} = 12.7, and pK_a-Sr^{2+} = 13.2),[83] whereas the pK_a value of the Cd^{2+}-aqua ion was found to be 9.2.[83] This difference in the acidity of the water binding the heterocation may have a significant impact on the hydrogen bond network around the metal cluster and, therefore, on the catalytic activity of PSII. Nevertheless, the pK_a values reported for several metal-aqua complexes in water solution could change significantly in the protein environment. To check this possibility, we estimated the relative pK_a of the water bound to the heterocation using the thermodynamic cycle shown in Figure 5. Assuming similar
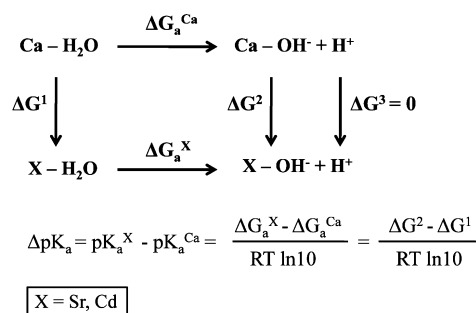

Figure 5. Thermodynamic cycle used for the determination of ΔpK_a.

entropic contributions for the three deprotonation reactions taken into account in this study, the relative pK_a can be evaluated by comparing the differences between the internal energy calculated for the three (relaxed) structures with the water molecule and that for the three (relaxed) structures with a hydroxide ion bound to the respective heterocation.

As shown in Table 2, the ΔpK_a of the Sr^{2+} with respect to the Ca^{2+} ion varies from ~0.5 in a water solution to ~1.0 as calculated in the OEC, while on the other side, the ΔpK_a between the Ca^{2+}-aqua ion and the Cd^{2+}-aqua ion, which was experimentally found to be approximately −3.5 in the water solution, increases to approximately −5.2 in the complex environment. Our results confirm that the trend of the acidity

Table 2. Relative pK_a Values of the Water Bound to the Heterocation[a]

heterocation	pK_a water[83]	ΔpK_a water[83]	ΔpK_a PSII
Ca^{2+}	12.67	—	—
Sr^{2+}	13.18	+0.51	+1.01
Cd^{2+}	9.2	−3.47	−5.25

[a]Calculations were performed in the gas phase by optimizing the systems in their respective protonation state.

characterizing the three investigated ions in water solution is still valid in PSII.

Though we did not calculate the absolute pK_a values for the three investigated cases, the relative pK_a values found in this study clearly suggest that the water bound to the Cd^{2+} ion can be more easily found in its deprotonated state than the respective water bound to the Ca^{2+} ion.

CONCLUSIONS

In this work, we investigated by means of gas-phase and QM/MM calculations the effect of the substitution of the Ca^{2+} ion in the oxygen-evolving complex of PSII with either Sr^{2+} or Cd^{2+} ion in the S_2 state of the Kok−Joliot cycle. Whereas the Sr^{2+} ion is experimentally known to restore the catalytic function of PSII in the calcium-depleted oxygen-evolving complex, albeit with a different turnover rate, Cd^{2+}-substituted PSII showed no activity, the catalytic cycle being stopped between the S_2 and S_3 states.[29] The calculated bond distances characterizing all the investigated heterocation-substituted models did not show significant variations for the different models, with both the coordinated water molecules and ligands minimally affected by the heterocation substitution. We additionally estimated the transition energy between the two open and closed cubane conformers representative of the S_2 state of the Kok−Joliot cycle, giving similar transition energies for the Ca^{2+} system and the two Sr^{2+}- and Cd^{2+}-substituted systems. As already seen in the case of the Mn_4CaO_5 cluster, also in the presence of Sr^{2+} or Cd^{2+} ion, the oxidation of Mn(III) by the Tyr-Z radical was found to occur in the closed cubane conformation during QM/MM molecular dynamics simulations on the picosecond time scale, as also suggested by PDOS analysis. Under the conditions adopted in our simulations, from the structural and electronic point of view, both Sr^{2+}- and Cd^{2+}-substituted PSII should reveal catalytic activity or at least should reach the S_3 state of the Kok−Joliot cycle. Nevertheless, a crucial issue in our simulations is the assumption that the hydrogen bond and the protonation patterns of the binding pocket do not depend on the divalent cation, being in all cases identical to those of wild-type PSII. To investigate this issue, we performed single-point energy calculations to characterize the pK_a differences of the water molecule bound to the respective heterocations. Our calculations reported a ΔpK_a of approximately +1.0 in the case of Sr-substituted PSII and a ΔpK_a of approximately −5.3 in the case of Cd-substituted PSII. This large difference in acidity suggests that the water directly bound to the Cd^{2+} ion can be easily found as a hydroxide ion. Different protonation states of the water molecules around the heterocations may severely change the hydrogen bonding network around the manganese cluster and Tyr-Z, therefore influencing the redox potential levels involved in the passage between the S_2 and S_3 states. It has recently been shown in inorganic clusters mimicking the Mn_4CaO_5 core[58] that redox-inactive metals can have a large influence on the redox properties of bound redox-active ions.

The same rationale might also be applied for the PSII core. Taken together, our results lend support to the idea of a structural role for the Ca^{2+} ion that can be fulfilled by several ions until the S_2 state, where the access to the final steps of the Kok−Joliot cycle can be accomplished by only cations characterized by a similar Lewis acidity, which was also suggested as the basis of the pK_a values of the cations in water solutions by Brudvig and co-workers.[24,29,39] Finally, we have also found that the position of the lowest unoccupied molecular orbital projected on Tyr-Z in both the Sr^{2+}- and Cd^{2+}-substituted systems is influenced by the heterocation, being at lower energies when compared with the Mn_4CaO_5 case. The nature of the cation can therefore also have a direct influence on the oxidation potential of Tyr-Z, beyond the effect mediated by the local hydrogen bond network rearrangement as also pointed out previously.[57]

AUTHOR INFORMATION

Corresponding Author

*E-mail: leonardo.guidoni@univaq.it.

Notes

The authors declare no competing financial interest.

ABBREVIATIONS

PSII, photosystem II; OEC, oxygen-evolving complex; QM/MM, quantum mechanics/molecular mechanics; GP, gas phase; MD, molecular dynamics; PDOS, projected density of states; OC, open cubane; CC, closed cubane; EPR, electron paramagnetic resonance; HOMO, highest occupied molecular orbital; LUMO, lowest unoccupied molecular orbital.

REFERENCES

(1) Barber, J. (2009) Photosynthetic energy conversion: natural and artificial. *Chem. Soc. Rev. 38*, 185−196.

(2) Kok, B., Forbush, B., and McGloin, M. (1970) Cooperation of charges in photosynthetic O2 evolution. *Photochem. Photobiol. 11*, 457−475.

(3) Nocera, D. G. (2012) The Artificial Leaf. *Acc. Chem. Res. 45*, 767−776.

(4) Faunce, T., et al. (2013) Artificial photosynthesis as a frontier technology for energy sustainability. *Energy Environ. Sci. 6*, 1074−1076.

(5) Yehezkeli, O., Tel-Vered, R., Wasserman, J., Trifonov, A., Michaeli, D., Nechushtai, R., and Willner, I. (2012) Integrated photosystem II-based photo-bioelectrochemical cells. *Nat. Commun. 3*, 742.

(6) Kanan, M. W., and Nocera, D. G. (2008) In Situ Formation of an Oxygen-Evolving Catalyst in Neutral Water Containing Phosphate and Co^{2+}. *Science 321*, 1072−1075.

(7) Kanan, M. W., Surendranath, Y., and Nocera, D. G. (2009) Cobalt-phosphate oxygen-evolving compound. *Chem. Soc. Rev. 38*, 109−114.

(8) Robblee, J. H., Cinco, R. M., and Yachandra, V. K. (2001) X-ray spectroscopy-based structure of the Mn cluster and mechanism of photosynthetic oxygen evolution. *Biochim. Biophys. Acta, Bioenerg. 1503*, 7−23.

(9) Yano, J., Kern, J., Sauer, K., Latimer, M. J., Pushkar, Y., Biesiadka, J., Loll, B., Saenger, W., Messinger, J., Zouni, A., and Yachandra, V. K.

(2006) Where water is oxidized to dioxygen: structure of the photosynthetic Mn_4Ca cluster. *Science 314*, 821−825.

(10) Dau, H., Grundmeier, A., Loja, P., and Haumann, M. (2008) On the structure of the manganese complex of photosystem II: extended-range EXAFS data and specific atomic-resolution models for four S-states. *Philos. Trans. R. Soc., B 363*, 1237−1243.

(11) Pushkar, Y., Yano, J., Sauer, K., Boussac, A., and Yachandra, V. K. (2008) Structural changes in the Mn_4Ca cluster and the mechanism of photosynthetic water splitting. *Proc. Natl. Acad. Sci. U. S. A. 105*, 1879−1884.

(12) Zouni, A., Witt, H. T., Kern, J., Fromme, P., Krauss, N., Saenger, W., and Orth, P. (2001) Crystal structure of photosystem II from Synechococcus elongatus at 3.8 Å resolution. *Nature 409*, 739−743.

(13) Loll, B., Kern, J., Saenger, W., Zouni, A., and Biesiadka, J. (2005) Towards complete cofactor arrangement in the 3.0 Å resolution structure of photosystem II. *Nature 438*, 1040−1044.

(14) Guskov, A., Kern, J., Gabdulkhakov, A., Broser, M., Zouni, A., and Saenger, W. (2009) Cyanobacterial photosystem II at 2.9 Å resolution and the role of quinones, lipids, channels and chloride. *Nat. Struct. Mol. Biol. 16*, 334−342.

(15) Umena, Y., Kawakami, K., Shen, J.-R., and Kamiya, N. (2011) Crystal structure of oxygen-evolving photosystem II at a resolution of 1.9 Å. *Nature 473*, 55−60.

(16) Siegbahn, P. E. M. (2011) Recent theoretical studies of water oxidation in photosystem II. *J. Photochem. Photobiol., B 104*, 94−99.

(17) Galstyan, A., Robertazzi, A., and Knapp, E. W. (2012) Oxygen-Evolving Mn Cluster in Photosystem II: The Protonation Pattern and Oxidation State in the High-Resolution Crystal Structure. *J. Am. Chem. Soc. 134*, 7442−7449.

(18) Kurashige, Y., Chan, G. K., and Yanai, T. (2013) Entangled quantum electronic wavefunctions of the Mn_4CaO_5 cluster in photosystem II. *Nat. Chem. 5*, 660−666.

(19) Siegbahn, P. E. M. (2013) Water oxidation mechanism in photosystem II, including oxidations, proton release pathways, O-O bond formation and O_2 release. *Biochim. Biophys. Acta, Bioenerg. 1827*, 1003−1019.

(20) Saito, K., Rutherford, A. W., and Ishikita, H. (2013) Mechanism of proton-coupled quinone reduction in Photosystem II. *Proc. Natl. Acad. Sci. U. S. A. 110*, 954−959.

(21) Suga, M., Akita, F., Hirata, K., Ueno, G., Murakami, H., Nakajima, Y., Shimizu, T., Yamashita, K., Yamamoto, M., Ago, H., and Shen, J.-R. (2014) Native structure of photosystem II at 1.95 Å resolution viewed by femtosecond X-ray pulses. *Nature 517*, 99−103.

(22) Miqyass, M., van Gorkom, H. J., and Yocum, C. F. (2007) The PSII calcium site revisited. *Photosynth. Res. 92*, 275−287.

(23) Boussac, A., Rappaport, F., Carrier, P., Verbavatz, J.-M., Gobin, R., Kirilovsky, D., Rutherford, A. W., and Sugiura, M. (2004) Biosynthetic Ca^{2+}/Sr^{2+} exchange in the photosystem II oxygen-evolving enzyme of Thermosynechococcus elongatus. *J. Biol. Chem. 279*, 22809−22819.

(24) Vrettos, J. S., Stone, D. A., and Brudvig, G. W. (2001) Quantifying the Ion Selectivity of the Ca^{2+} Site in Photosystem II:? Evidence for Direct Involvement of Ca^{2+} in O2 Formation. *Biochemistry 40*, 7937−7945.

(25) Ono, T. A., Rompel, A., Mino, H., and Chiba, N. (2001) Ca^{2+} Function in Photosynthetic Oxygen Evolution Studied by Alkali Metal Cations Substitution. *Biophys. J. 81*, 1831−1840.

(26) Ono, T. A., and Inoue, Y. (1989) Removal of Ca by pH 3.0 treatment inhibits S2 to S3 transition in photosynthetic oxygen evolution system. *Biochim. Biophys. Acta, Bioenerg. 973*, 443−449.

(27) van Oort, B., Kargul, J., Barber, J., and van Amerongen, H. (2014) Fluorescence kinetics of PSII crystals containing Ca^{2+} or Sr^{2+} in the oxygen evolving complex. *Biochim. Biophys. Acta, Bioenerg. 1837*, 264−269.

(28) Chatterjee, R., Milikisiyants, S., Coates, C. S., Koua, F. H. M., Shen, J.-R., and Lakshmi, K. V. (2014) The structure and activation of substrate water molecules in Sr^{2+}-substituted photosystem II. *Phys. Chem. Chem. Phys. 16*, 20834−20843.

(29) Lee, C., Lakshmi, K., and Brudvig, G. (2007) Probing the Functional Role of Ca^{2+} in the Oxygen-Evolving Complex of Photosystem II by Metal Ion Inhibition. *Biochemistry 46*, 3211−3223.

(30) Yocum, C. (2008) The calcium and chloride requirements of the O_2 evolving complex. *Coord. Chem. Rev. 252*, 296−305.

(31) Lohmiller, T., Shelby, M., Long, X., Yachandra, V. J. (2015) Removal of Ca^{2+} from the Oxygen-Evolving Complex in Photosystem II Has Minimal Effect on the Mn_4O_5 Core Structure: A Polarized Mn X-ray Absorption Spectroscopy Study. *J. Phys. Chem. B*, in press.

(32) Siegbahn, P., and Lundberg, M. (2006) Hydroxide instead of bicarbonate in the structure of the oxygen evolving complex. *J. Inorg. Biochem. 100*, 1035−1040.

(33) Cox, N., Rapatskiy, L., Su, J.-H., Pantazis, D. A., Sugiura, M., Kulik, L., Dorlet, P., Rutherford, A. W., Neese, F., Boussac, A., Lubitz, W., and Messinger, J. (2011) Effect of Ca^{2+}/Sr^{2+} Substitution on the Electronic Structure of the Oxygen-Evolving Complex of Photosystem II: A Combined Multifrequency EPR, 55Mn-ENDOR, and DFT Study of the S2 State. *J. Am. Chem. Soc. 133*, 3635−3648.

(34) Terrett, R., Petrie, S., Pace, R. J., and Stranger, R. (2014) What does the Sr-substituted 2.1 Å resolution crystal structure of photosystem II reveal about the water oxidation mechanism? *Chem. Commun. 50*, 3187−3190.

(35) Siegbahn, P. (2014) Water oxidation energy diagrams for photosystem II for different protonation states, and the effect of removing calcium. *Phys. Chem. Chem. Phys. 16*, 11893−11900.

(36) Vogt, L., Ertem, M. Z., Pal, R., Brudvig, G. W., and Batista, V. S. (2015) Computational Insights on Crystal Structures of the Oxygen-Evolving Complex of Photosystem II with Either Ca^{2+} or Ca^{2+} Substituted by Sr^{2+}. *Biochemistry 54*, 820−825.

(37) Haddy, A. (2007) EPR spectroscopy of the manganese cluster of photosystem II. *Photosynth. Res. 92*, 357−368.

(38) Koua, F. H. M., Umena, Y., Kawakami, K., and Shen, J.-R. (2013) Structure of Sr-substituted photosystem II at 2.1 Å resolution and its implications in the mechanism of water oxidation. *Proc. Natl. Acad. Sci. U. S. A. 110*, 3889−3894.

(39) Brudvig, G. (2008) Water oxidation chemistry of photosystem II. *Philos. Trans. R. Soc., B 363*, 1211−1219.

(40) Nilsson, H., Rappaport, F., Boussac, A., and Messinger, J. (2014) Substrate-water exchange in photosystem II is arrested before dioxygen formation. *Nat. Commun. 5*, 4305.

(41) Matysik, J., Alia, A., Nachtegaal, G., van Gorkom, H. J., Hoff, A. J., and de Groot, H. J. M. (2000) Exploring the Calcium-Binding Site in Photosystem II Membranes by Solid-State 113Cd NMR. *Biochemistry 39*, 6751−6755.

(42) Waggoner, C., and Yocum, C. (1990) in *Current Research in Photosynthesis* (Baltscheffsky, M., Ed.) pp 733−736, Springer, Dordrecht, The Netherlands.

(43) Rutherford, A., and Faller, P. (2001) The heart of photosynthesis in glorious 3D. *Trends Biochem. Sci. 26*, 341−344.

(44) de Odrowaaz Piramowicz, M., Bock, R., Orzechowska, A., Strzałka, K., and Burda, K. (2008) *Photosynthesis. Energy from the Sun*, pp 311−314, Springer, Berlin.

(45) Geiken, B., Masojidek, J., Rizzuto, M., Pompili, M., and Giardi, M. (1998) Incorporation of [35S] methionine in higher plants reveals that stimulation of the D1 reaction centre II protein turnover accompanies tolerance to heavy metal stress. *Plant, Cell Environ. 21*, 1265−1273.

(46) Franco, E., Alessandrelli, S., Masojídek, J., Margonelli, A., and Giardi, M. T. (1999) Modulation of D1 protein turnover under cadmium and heat stresses monitored by [35S]methionine incorporation. *Plant Sci. 144*, 53−61.

(47) Keller, S., Beatty, J. T., Paddock, M., Breton, J., and Leibl, W. (2001) Effect of metal binding on electrogenic proton transfer associated with reduction of the secondary electron acceptor (QB) in Rhodobacter sphaeroides chromatophores. *Biochemistry 40*, 429−439.

(48) Paddock, M., Graige, M., Feher, G., and Okamura, M. (1999) Identification of the proton pathway in bacterial reaction centers:

inhibition of proton transfer by binding of Zn^{2+} or Cd^{2+}. *Proc. Natl. Acad. Sci. U. S. A. 96*, 6183−6188.

(49) Ishikita, H., and Knapp, E.-W. (2005) Induced conformational changes upon Cd^{2+} binding at photosynthetic reaction centers. *Proc. Natl. Acad. Sci. U. S. A. 102*, 16215−16220.

(50) Axelrod, H., Abresch, E., Paddock, M., Okamura, M., and Feher, G. (2000) Determination of the binding sites of the proton transfer inhibitors Cd^{2+} and Zn^{2+} in bacterial reaction centers. *Proc. Natl. Acad. Sci. U. S. A. 97*, 1542−1547.

(51) Paddock, M., Sagle, L., Tehrani, A., Beatty, J., Feher, G., and Okamura, M. (2003) Mechanism of Proton Transfer Inhibition by Cd^{2+} Binding to Bacterial Reaction Centers: Determination of the pK_a of Functionally Important Histidine Residues. *Biochemistry 42*, 9626−9632.

(52) Sigfridsson, K. G., Bernát, G., Mamedov, F., and Styring, S. (2004) Molecular interference of Cd^{2+} with Photosystem II. *Biochim. Biophys. Acta, Bioenerg. 1659*, 19−31.

(53) Pantazis, D. A., Ames, W., Cox, N., Lubitz, W., and Neese, F. (2012) Two Interconvertible Structures that Explain the Spectroscopic Properties of the Oxygen-Evolving Complex of Photosystem II in the S_2 State. *Angew. Chem., Int. Ed. 51*, 9935−9940.

(54) Bovi, D., Narzi, D., and Guidoni, L. (2013) The S_2 State of the Oxygen-Evolving Complex of Photosystem II Explored by QM/MM Dynamics: Spin Surfaces and Metastable States Suggest a Reaction Path Towards the S_3 State. *Angew. Chem., Int. Ed. 52*, 11744−11749.

(55) Narzi, D., Bovi, D., and Guidoni, L. (2014) Pathway for Mn-cluster oxidation by tyrosine-Z in the S_2 state of photosystem II. *Proc. Natl. Acad. Sci. U. S. A. 111*, 8723−8728.

(56) Boussac, A., and Rutherford, A. W. (1988) Nature of the inhibition of the oxygen-evolving enzyme of photosystem II induced by sodium chloride washing and reversed by the addition of calcium(2+) or strontium(2+). *Biochemistry 27*, 3476−3483.

(57) Retegan, M., Cox, N., Lubitz, W., Neese, F., and Pantazis, D. A. (2014) The first tyrosyl radical intermediate formed in the S2-S3 transition of photosystem II. *Phys. Chem. Chem. Phys. 16*, 11901−11910.

(58) Tsui, E. Y., and Agapie, T. (2013) Reduction potentials of heterometallic manganese-oxido cubane complexes modulated by redox-inactive metals. *Proc. Natl. Acad. Sci. U. S. A. 110*, 10084−10088.

(59) Bang, S., Lee, Y., Hong, S., Cho, K., Nishida, Y., Seo, M., Sarangi, R., Fukuzumi, S., and Nam, W. (2014) Redox-inactive metal ions modulate the reactivity and oxygen release of mononuclear non-haem iron(III)-peroxo complexes. *Nat. Chem. 6*, 934−940.

(60) Ames, W., Pantazis, D. A., Krewald, V., Cox, N., Messinger, J., Lubitz, W., and Neese, F. (2011) Theoretical Evaluation of Structural Models of the S-2 State in the Oxygen Evolving Complex of Photosystem II: Protonation States and Magnetic Interactions. *J. Am. Chem. Soc. 133*, 19743−19757.

(61) Bovi, D., Narzi, D., and Guidoni, L. (2014) Magnetic interactions in the catalyst used by nature to split water: a DFT+U multiscale study on the Mn_4CaO_5 core in Photosystem II. *New J. Phys. 16*, 015020.

(62) Neese, F. (2012) The ORCA program system. *Wiley Interdisciplinary Reviews: Computational Molecular Science 2*, 73−78.

(63) Becke, A. D. (1988) Density-functional exchange-energy approximation with correct asymptotic behavior. *Phys. Rev. A: At., Mol., Opt. Phys. 38*, 3098−3100.

(64) Lee, C., Yang, W., and Parr, R. G. (1988) Development of the Colle-Salvetti correlation-energy formula into a functional of the electron density. *Phys. Rev. B: Condens. Matter Mater. 37*, 785−789.

(65) Becke, A. D. (1993) Density-Functional Thermochemistry 0.3. The role of exact exchange. *J. Chem. Phys. 98*, 5648−5652.

(66) Schäfer, A., Horn, H., and Ahlrichs, R. (1992) Fully optimized contracted Gaussian basis sets for atoms Li to Kr. *J. Chem. Phys. 97*, 2571−2577.

(67) Weigend, F. (2006) Accurate Coulomb-fitting basis sets for H to Rn. *Phys. Chem. Chem. Phys. 8*, 1057−1065.

(68) Sinnecker, S., Rajendran, A., Klamt, A., Diedenhofen, M., and Neese, F. (2006) Calculation of solvent shifts on electronic g-tensors with the conductor-like screening model (COSMO) and its self-consistent generalization to real solvents (Direct COSMO-RS). *J. Phys. Chem. A 110*, 2235−2245.

(69) Pantazis, D. A., Chen, X.-Y., Landis, C. R., and Neese, F. (2008) All-electron scalar relativistic basis sets for third-row transition metal atoms. *J. Chem. Theory Comput. 4*, 908−919.

(70) VandeVondele, J., Krack, M., Mohamed, F., Parrinello, M., Chassaing, T., and Hutter, J. (2005) QUICKSTEP: Fast and accurate density functional calculations using a mixed gaussian and plane waves approach. *Comput. Phys. Commun. 167*, 103−128.

(71) Laino, T., Mohamed, F., Laio, A., and Parrinello, M. (2005) An efficient real space multigrid QM/MM electrostatic coupling. *J. Chem. Theory Comput. 1*, 1176−1184.

(72) Goedecker, S., Teter, M., and Hutter, J. (1996) Separable dual-space Gaussian pseudopotentials. *Phys. Rev. B: Condens. Matter Mater. Phys. 54*, 1703−1710.

(73) Hartwigsen, C., Goedecker, S., and Hutter, J. (1998) Relativistic separable dual-space Gaussian Pseudopotentials from H to Rn. *Phys. Rev. B: Condens. Matter Mater. Phys. 58*, 3641−3662.

(74) VandeVondele, J., and Hutter, J. (2007) Gaussian basis sets for accurate calculations on molecular systems in gas and condensed phases. *J. Chem. Phys. 127*, 114105.

(75) Perdew, J. P., Burke, K., and Ernzerhof, M. (1996) Generalized gradient approximation made simple. *Phys. Rev. Lett. 77*, 3865−3868.

(76) Dudarev, S. L., Manh, D. N., and Sutton, A. P. (1997) Effect of Mott-Hubbard correlations on the electronic structure and structural stability of uranium dioxide. *Philos. Mag. B 75*, 613−628.

(77) Dudarev, S. L., Botton, G. A., Savrasov, S. Y., Humphreys, C. J., and Sutton, A. P. (1998) Electron-energy-loss spectra and the structural stability of nickel oxide: An LSDA+U study. *Phys. Rev. B: Condens. Matter Mater. Phys. 57*, 1505−1509.

(78) Hoover, W. G. (1985) Canonical dynamics: Equilibrium phase-space distribution. *Phys. Rev. A: At., Mol., Opt. Phys. 31*, 1695−1697.

(79) Nosé, S. (1984) A unified formulation of the constant temperature molecular dynamics methods. *J. Chem. Phys. 81*, 511−519.

(80) Nosé, S. (1984) A molecular dynamics method for simulation in the canonical ensemble. *Mol. Phys. 52*, 255−268.

(81) Siegbahn, P. E. M. (2006) The performance of hybrid DFT for mechanisms involving transition metal complexes in enzymes. *JBIC, J. Biol. Inorg. Chem. 11*, 695−701.

(82) Cox, N., and Messinger, J. (2013) Reflections on substrate water and dioxygen formation. *Biochim. Biophys. Acta, Bioenerg. 1827*, 1020−1030.

(83) Dean, J. A. (1999) *Lange's Handbook of chemistry*, 15th ed., McGraw-Hill, New York.